Towards a better understanding of the evaporative cooling of rivers: case study for the Little Southwest Miramichi River (New Brunswick, Canada)

Valerie Ouellet[a] and Daniel Caissie[b*]

[a]Integrated Statistics contractor for NOAA's Northeast Fisheries Science Center, Orono, ME; [b] Fisheries and Oceans, Moncton, NB, Canada, E1C 9B6

Corresponding author email**:** **Daniel.Caissie@dfo-mpo.gc.ca**

ORCID ID: Ouellet = 0000-0001-7410-1857; Caissie = 0000-0002-4405-4639

Biographical notes:

Ouellet: Dr. Ouellet is a diadromous fish scientist for Integrated Statistics Inc, supporting NOAA Northeast Fisheries Sciences Center. Her primary interest regards understanding how different environmental variables, such as water temperature and flow, affect the habitat of key fish species. She worked on thermal budgets, water temperature, and fish habitat modeling using a variety of quantitative approaches. She focuses on fundamental questions about the relationship between stream hydrology, thermal regimes, and fish physiology and habitat. She is also interested in large-scale research and management targeting diadromous species. Her research aims to generate knowledge critical to improve large-scale conservation and ecosystem restoration, especially regarding climate change.

Caissie: Dr. Caissie is a scientist emeritus research hydrologist for the department within the Freshwater Habitat Section in Moncton, NB. He has been part of the Catamaran Brook Habitat Research Project, and has published extensively in the field of hydrology and fish habitat. His main research interests are: the understanding the thermal regime of rivers and river heat fluxes, stream temperature modeling, instream flow requirements, statistical hydrology (floods and droughts), river hydraulics and anthropogenic impacts. He has taught both river hydrology and river hydraulics courses at Université de Moncton.

Towards a better understanding of the evaporative cooling of rivers: case study for the Little Southwest Miramichi River (New Brunswick, Canada)

Abstract

Stream temperature plays an important role in many biotic and abiotic processes, as it influences many physical, chemical, and biological properties in rivers. As such, a good understanding of the thermal regime of rivers is essential for effective fisheries management and the protection of aquatic habitats. Moreover, a thorough understanding of underlying physical processes and river heat fluxes is essential in developing better and more adaptive water temperature models. Very few studies have quantified river evaporation and rivers' corresponding evaporative cooling component. The present study investigated the evaporative cooling of the Little Southwest Miramichi River in Eastern Canada by calculating the evaporative heat flux and overall heat fluxes using in-situ data. Results showed that the evaporative heat flux reached -300 W m^{-2} mid-day when high water temperatures were observed. The daily evaporative heat flux can thus account for close to 50% of the total heat losses, followed by longwave radiation (25%), streambed heat fluxes (20%), and sensible heat (5%). Our results show that the evaporative heat flux can be a critical cooling mechanism for wide and shallow rivers during high summer temperatures.

KEYWORDS: river; evaporation; heat flux; Dalton-type approach, water temperature

1. Introduction

River temperature is a critical parameter in ecological studies as it influences many physical, chemical, and biological processes. For instance, river temperature can impact fish distribution, growth rates, mortality, and habitat use within river systems (Svenning et al. 2022; Armstrong et al. 2013; Elliot and Hurley 2000; Keefer, Peery, and High 2009; Ouellet et al. 2021). Aquatic species distribution can also be influenced by seasonal, daily, and diel water temperature variability, which can differ significantly between small groundwater-fed streams and large rivers (Tague et al. 2008; Hare et al. 2021; Kurylyk et al. 2015). An important component of the overall thermal regime of rivers is the occurrence of high temperature events (Caissie et al. 2013), which can severely impact fish behavior and their distribution (Breau, Weir, and Grant 2007; Breau, Cunjak, and Peake 2011; Corey et al. 2020). For example, under high temperatures, salmonids have been observed to experience stress-related responses (Elvidge et al. 2017; Corey et al. 2017; Kingsolver, Diamond, and Buckley 2013), including the movement of fishes into small cold-water tributaries to seek thermal refugia (Petty et al. 2014; Frechette et al. 2018; Dugdale et al. 2015). In extreme cases, high temperature events can result in direct fish mortalities (Huntsman 1942; Ouellet et al. 2010). As river temperature plays a major role in aquatic resources composition and distribution, it is therefore imperative to understand the spatial and temporal variability of the underlying physical processes for improved modeling and more effective fisheries and aquatic resources management (Dugdale et al. 2018; Ouellet et al. 2020).

Among the best approach to understand river thermal processes is to quantify the heat exchanges within river environments, as statistical river temperature models do not provide such information. As such, river temperature heat budget models are often used to quantify heat fluxes to predict water temperatures under natural conditions and anthropogenic perturbations (Garner et al. 2014; Carrivick et al. 2012; Maheu et al. 2014; Ouellet et al. 2013). River temperature models can generally be classified

as statistical or deterministic/process-based (Caissie 2006; Benyahya et al. 2007). Statistical models are used to predict river temperatures from a limited number of independent variables, such as air temperature (Mohseni and Stefan 1999; Caissie, El-Jabi, and Satish 2001; Ahmadi-Nedushan et al. 2007). These models provide little understanding of physical forcing and processes as they are based on statistical relationships.

In contrast, deterministic models are based on the conservation of energy and as such, need to effectively quantify heat exchange processes within the river environment to predict water temperature variability (Ouellet et al. 2020; Dugdale, Hannah, and Malcolm 2017). From a river perspective, the heat exchange is considered at two levels (1) at the air/water interface and (2) at the streambed/water interface (or stream bottom). Many applications of deterministic models can be found within the literature where river temperature has been successfully modeled (Sinokrot and Stefan 1994; Hebert et al. 2011; Ouellet et al. 2013; Jackson et al. 2021; Palmer and Nelson 2007; Caissie, Satish, and El-Jabi 2007). Moreover, the deterministic modeling approach remains the most effective tool when studying specific heat budget components or when conducting thermal impact studies (Troxler and Thackston 1977; Hockey, Owens, and Tapper 1982; Lowney 2000; Jackson et al. 2021). However, it is worth mentioning that deterministic models require more data in their application, e.g., detailed physiographic, hydrologic, and meteorological inputs (Ouellet et al. 2020; Dugdale, Hannah, and Malcolm 2017).

River heat exchange processes are complex and occur through a combination of radiation, conduction, convection, and advection processes (Garner et al. 2014; Dugdale, Hannah, and Malcolm 2020; Ouellet et al. 2013; Leach and Moore 2018). Energy fluxes at the air/water interface generally include solar radiation, net longwave radiation, and evaporative and sensible heat fluxes, whereas streambed heat fluxes mainly consist of heat conduction and advective processes (e.g., due to groundwater flow). Among the river heat budget components, the evaporative heat flux is important, as

it contributes to the cooling of rivers during high summer temperatures (Benyahya et al. 2010; Maheu et al. 2014). However, this heat flux has received very little attention within the literature and remains generally poorly understood, especially for rivers that can experience high summer water temperatures. Very few studies have used river-specific equations to quantify the evaporative heat flux (Guenther, Moore, and Gomi 2012; Caissie 2006; Ouellet et al. 2014). Many studies have calculated heat fluxes using literature equations developed for streams within very different climates and geographic settings (Caissie, Satish, and El-Jabi 2007; Sinokrot and Stefan 1994; Webb and Zhang 2004; Ouellet et al. 2014). However, the influence of hydrogeological settings (e.g., bedrock, surficial geology, soil types) that control river's thermal capacity and hydraulic conductivity are often overlooked, and heat fluxes are assumed constants or defined more arbitrarily (O'Sullivan, Devito, and Curry 2019; O'Sullivan et al. 2020; Jackson et al. 2021). This can explain why studies have observed large differences in evaporative heat fluxes when comparing different literature equations and the difficulty of extracting the information about coefficient adjustments (Benyahya et al. 2010; Ouellet et al. 2014). For example, Benyahya et al. (2010) used four different evaporation equations, and results showed that the Priestley–Taylor, and Penman equations generally showed higher evaporation rates than Dalton-type approach and the Ryan–Harleman equations.

Among these four evaporation equations, the Dalton-type equation is the most often used equation in water temperature modeling studies. When used, Dalton-type equations are often applied uncalibrated (i.e., using literature coefficients/equations) or calibrated using the energy-budget approach (Jobson 1980; Fulford and Sturm 1984) rather than actual evaporation measurements. However, in recent years some studies have made progress in direct river evaporation in order to better estimate the wind function when using the Dalton-type approach (Guenther, Moore, and Gomi 2012; Maheu et al. 2014; Caissie 2016). For example, Guenther et al. (2012) measured evaporation rates in a small

headwater stream in British Columbia using an evaporimeter, whereas both Maheu et al. (2014) and Caissie (2016) have used floating minipans to calibrate their Dalton-type equations. Maheu et al. (2014) have quantified river evaporation for two different size rivers and found differences in the wind function at each site. Notably, site-specific equations should be used whenever possible, as they likely better reflect river evaporation than literature equations. Site-specific equations can improve the evaporative heat flux estimation and thus can contribute to a better overall modeling. Also, site-specific equations can play an important role in our ability to generalize the evaporative heat flux component in the future, which would be the ultimate goal. Although Maheu et al. (2014) have established river-specific wind functions, calculated river evaporation, and corresponding heat fluxes, their study focused mainly on river evaporation. In the present study, the focus is on the evaporative heat flux at daily and diel timescales to better assess the evaporative cooling potential of rivers (i.e., the percentage/portion of the evaporative heat flux among the total heat losses). The evaporative cooling of rivers can plays a key role in warm and cold climates where rivers are experiencing high summer temperatures, such as the Little Southwest Miramichi River which can reaching 30°C. Such rivers may be further impacted under future climate warming.

The present study will quantify the evaporative heat flux as well as the evaporative cooling (i.e., the percentage of the evaporative heat flux to the total heat losses) within the Little Southwest Miramichi River (New Brunswick, Canada). The specific objectives of this research are: 1) to use a Dalton-type approach to calculate the river evaporation and the corresponding evaporative heat fluxes, 2) to compare the different heat fluxes (gains and losses) that contribute to the overall heat budget, and 3) to quantify the evaporative heat fluxes at both daily and diel timescale to assess potential evaporative cooling of the studied river.

2. Study sites and data

In the present study, data were collected within the lower section of the Little Southwest Miramichi River (LSWM), New Brunswick (Eastern Canada) (Figure 1). The drainage area at this site is 1190 $km^{2,}$ and the river is approximately 80 m wide, with a depth of 0.55 m (average depth during mean flow conditions). The LSWM is part of the Miramichi River system, which is world-renowned for its population of Atlantic salmon (DFO 2013). The study area receives between 860 mm and 1365 mm of precipitation annually, with a mean annual precipitation of 1130 mm (Caissie and El-Jabi 1995). The mean annual runoff is estimated at 714 mm, and 416 mm of the water is lost through evapotranspiration. January is the coldest month, with a mean monthly air temperature of -11.8°C, whereas July is the warmest month, with an average air temperature of 18.8°C. Conifers (65%) and some deciduous trees (35%) make up the predominant vegetation cover in the region (Cunjak, Caissie, and El-Jabi 1990). The canopy closure is less than 20% at LSWM, which is an estimate of shading of the river during mid-day, and the tallest mature trees are typically in the order of 14–18 m.

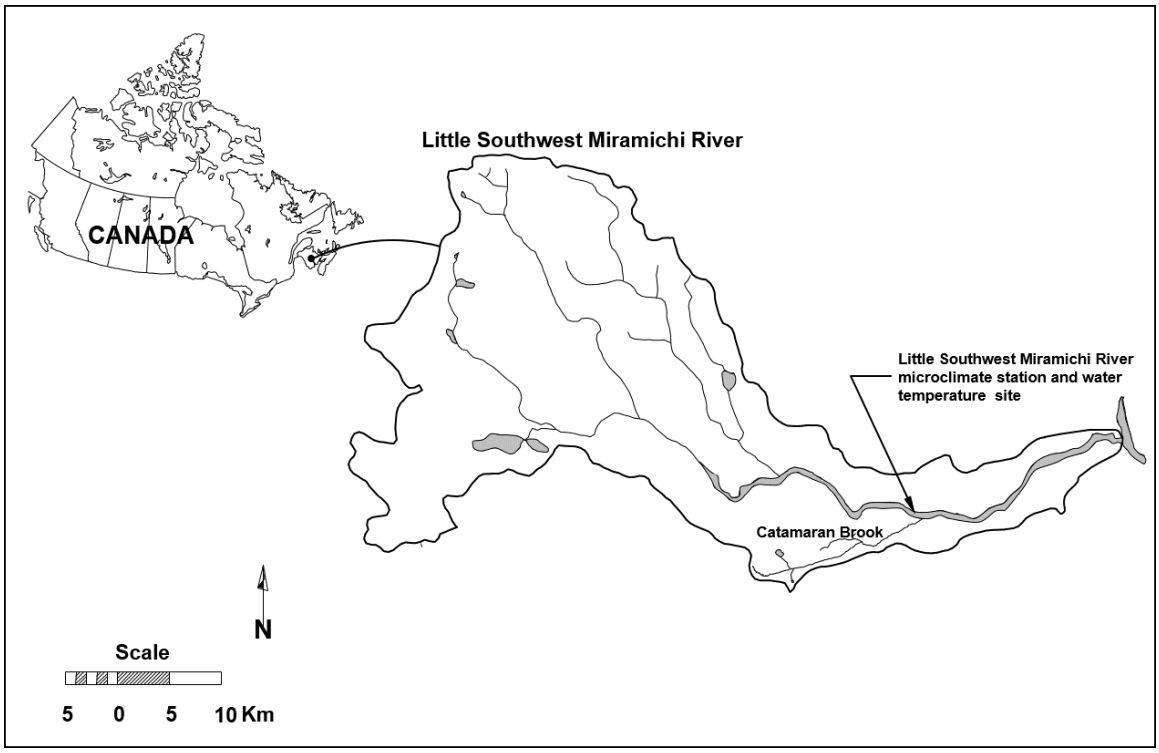

Figure 1. Little Southwest Miramichi River drainage basin indicating the location of the microclimate station and water temperature monitoring site.

For this study, data were collected within the Little Southwest Miramichi River, from instruments installed in the mid-stream environment just below the confluence of Catamaran Brook (Figure 1). Water temperature was recorded using a Campbell Scientific 107B water temperature sensor. No difference in water temperatures was observed from bank-to-bank due to the well-mixed nature of the river (Caissie, Satish, and El-Jabi 2007). Air temperature and relative humidity were measured 2 m above the water surface using a shielded Vaisala Relative Humidity and Temperature sensor. Wind speed was monitored with a RM Young sensor. Longwave radiation data were collected using a Kipp & Zonen CGR3 pyrgeometer to obtain incoming atmospheric longwave radiation. Solar radiation was measured with a Kipp & Zonen SP-Lite2 silicon pyranometer. Precipitation was also recorded using a TE525 tipping bucket rain gage. Hourly data from June 12, 2012 (day 164) to September 6, 2012 (day 250) were available for the analysis. River evaporation equations (wind functions) used in the present

study were obtained from Maheu et al. (2014). River discharge data for the Little Southwest Miramichi were obtained from the following web site (www.canada.ca/en/environment-climate-change/services/water-overview/quantity/monitoring/suvery.html) for the hydrometric station (01BP001). Discharge data from the hydrometric station were used to calculate water level using the prorating technique described by Caissie et al. (2007).

2.1 Estimation of surface and streambed heat fluxes

The governing equation for one-dimensional heat transfer and for a vertically well-mixed stream is expressed as follows (Caissie and Luce 2017; Younus, Hondzo, and Engel 2000):

$$\frac{\partial T_w}{\partial t} + v\frac{\partial T_w}{\partial x} - \frac{1}{A}\frac{\partial}{\partial x}\left(AD_L\frac{\partial T_w}{\partial x}\right) = \frac{W}{\rho_w c_w A}(H_{surf} - H_{cond}) \qquad (1)$$

where, T_w represents the water temperature (°C), t is the time (s), x is the distance downstream (m), A is the cross-sectional area (m^2), v is the mean water velocity (m s^{-1}), W is the river width (m), D_L is the dispersion coefficient in the direction of flow (m^2 s^{-1}), c_w is the specific heat of water (4187 J kg^{-1} $°C^{-1}$) and ρ_w is the water density (1000 kg m^{-3}). H_{surf} is the total heat flux from the atmosphere, i.e., heat exchange at the air-water interface (W m^{-2}), and H_{cond} is the streambed conduction heat flux (W m^{-2}), i.e., the heat flux across the stream–streambed interface. As pointed out by Caissie and Luce (2017), equation (1) assumes that the water moving up from the streambed (upwelling case) has time to equilibrate to the river stream temperature as it exits the bed and enters the stream.

The total surface heat flux is a function of:

$$H_{surf} = H_{sw} + H_{lw} + H_e + H_{sh} \quad (2)$$

where H_{sw} is the net shortwave radiation (W m^{-2}), H_{lw} represents the net longwave radiation (W m^{-2}), H_e is the evaporative heat flux (W m^{-2}), and H_{sh} is the sensible heat flux (W m^{-2}).

2.1.1 Net shortwave radiation (Hsw)

The net shortwave (solar) radiation (H_{sw}) at the river surface may be approximated by the following equation (Sinokort and Stefan, 1993; Caissie et al., 2007):

$$H_{sw} = F_c H_{swi} - R\, F_c H_{swi} \quad (3)$$

where, H_{swi} represents the incoming shortwave radiation (W m^{-2}) which is measured by a pyranometer (representing above the forest canopy solar radiation), and F_c is the forest cover factor (0 totally shaded to 1 totally open). Since the microclimate station was located near the center of the LSWM, the measured pyranometer data was used to estimate the incoming shortwave radiation, i.e., $H_{swi,}$ and the forest cover factor (F_c) was assumed to be 1, i.e., totally open. The reflected component (R) was assumed at 3% of the incoming shortwave radiation based on Benyahya et al. (2012), which showed R values ranging from 1-6% and a corresponding mean value of 3%. Other studies have reported values in the range of 3-5% (e.g., Leach and Moore 2010), which shows that 3% is within the observed values.

2.1.2 Net longwave radiation (H_{lw})

The net longwave radiation flux (H_{lw}) at the water surface includes the incoming longwave radiation ($H_{lw}\downarrow$) and the outgoing radiation ($H_{lw}\uparrow$). The net longwave radiation is given by:

$$H_{lw} = H_{lw}\downarrow - H_{lw}\uparrow \quad (4)$$

As the longwave radiation ($H_{lw}\downarrow$, W m^{-2}) was measured using a pyrgeometer approximately mid-river, it mainly included longwave radiation coming from the atmosphere (H_{lwa}), but could also included a small portion coming from the nearby forest canopy (H_{lwf}) if present (although the LSWM is wide and unsheltered). The outgoing longwave radiation, $H_{lw}\uparrow$ (W m^{-2}), includes the reflected longwave radiation (H_{lwr}), and the longwave radiation emitted by the water surface (H_{lws}). The outgoing longwave radiation emitted by the water surface was calculated using the Stefan-Boltzmann law given by:

$$H_{lws}\uparrow = \sigma\, \varepsilon_w\, (T_w + 273)^4 \quad (5)$$

where, σ is the Stefan-Boltzman constant (5.67×10^{-8} W m^{-2} K^{-4}), $\varepsilon_w = 0.97\pm0.005$ (Anderson 1954) is the emissivity of the water and T_w the water temperature (°C). As in previous studies (Anderson, 1954; Benyahya et al., 2012) the reflected longwave radiation was assumed at 3% of incoming, therefore:

$$H_{lwr}\uparrow = 0.03\, H_{lw}\downarrow \quad (6)$$

As such, H_{lwr} represented 3% of the measured value of the pyrgeometer, or incoming longwave radiation.

2.1.3 Evaporative heat flux (H_{evp})

The evaporative heat flux (also known as latent heat flux, H_{evp}) can be calculated by the equation provided in Webb and Zhang (1997):

$$H_{evp} = E\ L\ \rho \quad (7)$$

where, E is the river evaporation rate (mm d^{-1}), L is the latent heat of water vaporization (2.45 MJ kg^{-1}) and ρ the water density (1000 kg m^{-3}). If we use the Dalton-type approach equation to estimate the river evaporation then the evaporation is given by:

$$E = (a + b\,u_2)\,(e_s^* - e_a) \quad (8)$$

where E in mm d^{-1}, u_2 wind speed in m s^{-1} at a height of 2 m, e_s* is the saturation vapour pressure of the surface (water), and e_a is the air vapour pressure in kPa. The coefficients a and b are constants of the Dalton-type approach evaporation equation, which are site-specific. Also, the quantity (a + b u_2) of equation (8) is referred to as the wind function (ψ), whereas (e_s*-e_a) is referred to as the vapour pressure difference between water and air. In the present study, the equations developed by Maheu et al. (2014) for the Little Southwest Miramichi River were used for calculating the evaporative heat flux.

2.1.4 Sensible heat flux (H_{sh})

The sensible heat equation is derived from the Bowen Ratio B, which is the ratio of the sensible to the evaporative heat flux where both fluxes are in the same units (*e.g.*, W m^{-2}) (Vercauteren et al. 2009; Caissie, Satish, and El-Jabi 2007):

$$B = \frac{H_{sh}}{H_{evp}} \quad (9)$$

The Bowen ratio is also given by (Bowen 1926):

$$B = \gamma \frac{T_s - T_a}{e_s^* - e_a} \quad (10)$$

where γ is the psychometric constant, T_s the surface temperature (water, °C) and T_a the air temperature (°C). After simplifications, the sensible heat flux equation is given by:

$$H_{sh} = 1.91(a + b\,u_2)(T_a - T_w) \quad (11)$$

where, a and b are the coefficients of the wind function (see equation 8), u_2 is the wind speed (m s^{-1}) at 2 m, T_a and T_w are the air and water temperature ($T_s = T_w$; °C).

2.1.5 Streambed heat flux (H_{cond})

The streambed heat flux (i.e., at the stream-streambed interface) is obtained from the streambed conduction flux given by the following equation:

$$H_{cond} = -k \left.\frac{\partial T}{\partial z}\right|_{z=0} \quad (12)$$

where k is the thermal conductivity of the saturated sediment matrix (W m^{-1} °C^{-1}). H_{cond} is the conductive heat flux across the stream–streambed interface (z = 0; Hondzo, Stefan, and Anthony 1994). The streambed conduction heat flux is the only streambed heat flux present in most situations, especially when upwelling water has time to equilibrate to the stream temperature as it moves through the sediment-water matrix (Caissie and Luce, 2017). There are different approaches to calculating H_{cond} (i.e., through a flux separation when the vertical velocity is known); however, the simplest approach is to use shallow streambed temperatures and calculate the slope, i.e., $\left.\frac{\partial T}{\partial z}\right|_{z=0}$ of equation (12). In the

present study, this approach was used where shallow streambed temperatures were calculated using an advection-diffusion model (Caissie and Satish 2001). Both upper and lower boundary conditions are required to run above the advection-diffusion model. The upper boundary was the surface water temperature of the Little Southwest Miramichi River, whereas the lower boundary was a constant temperature of 6.3°C at a depth of 6 m (Caissie et al. 2014). An upwelling water flux (velocity) of -0.0025 m hr^{-1} was used, which is a typical value for such river systems (Caissie et al. 2014). Stream temperatures (0 m; measured river temperatures) and streambed temperatures (from the above calculations) at depths of 0.1 m, 0.2 m, 0.3 m, and 0.4 m were used and fitted to a 3rd order polynomial function to estimate the slope of the equation (12), and thus provided the streambed (conduction) heat fluxes.

3. Results

3.1 Meteorological data

Little Southwest Miramichi River (LSWM) microclimate conditions were collected during the period between June 12, 2012 (day 164) and September 6, 2012 (day 250), and results of hourly data are shown in Figure 2. Figure 2a shows the incoming shortwave radiation (measured from the pyranometer) and incoming longwave radiation (measured from the pyrgeometer). Hourly data showed the diel cycles in both shortwave and longwave radiation. Peak values of incoming solar radiation generally reached 900 W m^{-2} early in the season (days 164-172) and declined towards the end of the study period (e.g., < 800 W m^{-2} days 223-250). The mean value for incoming solar (shortwave) radiation for the period was 205 W $m^{-2,}$ with higher daily means at the beginning (~ 300 W m^{-2}) and lower daily means towards the end of the period (~ 150 W m^{-2}). Incoming longwave radiation generally ranged between 295 W m^{-2} and 430 W m^{-2}, with a mean value of 370 W m^{-2} for the study period. Notably, measured incoming longwave

radiation followed the air temperature diel cycle and was also influenced by cloud cover. For instance, higher daily mean values were observed on cloudy days (e.g., days 174-180; days 223-226), while greater diel variability was observed during clear/sunny days. Figure 2b shows the study period's air and water temperature times series. Air temperature ranged from 5°C to 31°C, with an overall mean air temperature of 18.7°C. Morning temperatures were low, especially at the beginning and toward the end of the study period (e.g., minimum temperatures of 5°C on days 169 and 246; Figure 2b). High air temperatures of 29-31°C were observed on several days (e.g., days 172, 194, 197, 213, 218, and 239-240) with corresponding high water temperatures. The diel pattern of water temperatures was similar to that of air temperatures but with reduced diel variability (Figure 2b). Water temperature ranged between 14.3°C and 27.9°C, with an overall mean water temperature of 20.6°C. The mean summer water temperature in the Little Southwest Miramichi River was higher than the mean air temperature (by 1.9°C; 20.6°C vs. 18.7°C). Figure 2c shows the daily river discharge as well as hourly precipitation data. Discharge was under baseflow condition (i.e., without precipitation; discharge < 20 $m^3 s^{-1}$) for most of the summer; however, it responded to precipitation events. For instance, the discharge increased from 10 $m^3 s^{-1}$ (day 173) to 107 $m^3 s^{-1}$ (day 180) following 146 mm of rain, which fell over 8 days between June 22 and June 30 (days 174-182).

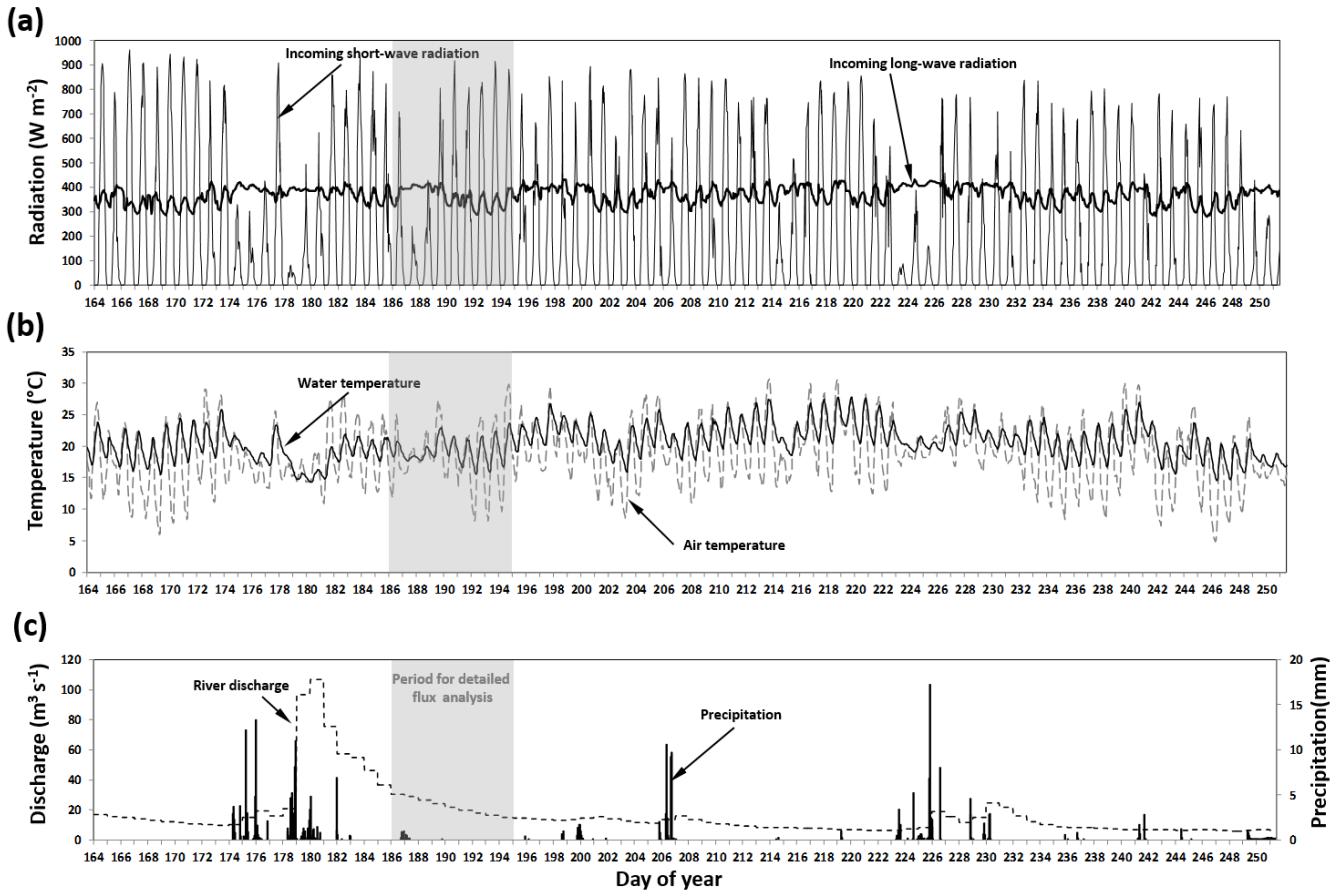

Figure 2. Meteorological data at the study site between June 12 (day 164) and September 6 (day 250), 2012. The shaded area indicates the period (July 4 to 13) for which the heat budget was analyzed in more detail.

It was possible to estimate the total heat flux (both at the air/water interface and the stream-streambed interface) using the above microclimate conditions and river discharge data. The period of July 4 to 13, 2012, (i.e., day of the year 186 to 195; shaded area; Figure 2) was used to illustrate these fluxes. This particular period was selected as it includes cloudy/overcast days, clear/sunny days, precipitation events, and high air temperature events (Figure 3; Table 1). For instance, days 186-188 were mainly overcast/cloudy days with some precipitation and were followed by days with a mix of sun and clouds (days 189-191; Table 1). The following two days were mainly clear days (days 192-193),

followed by a clear day where clouds moved in later in the day (day 194). The last day of the study period (day 195) experienced mostly cloudy conditions. Figure 3 shows the radiation components, air and water temperatures, wind speed, and relative humidity. During this period, 6.2 mm of precipitation was monitored on day 186 and early into day 187; however, this precipitation did not affect discharge which was in a recession flow condition from the previous high flow event (Figure 2). Both incoming shortwave radiation and longwave radiation are plotted in Figure 3a. Peak shortwave radiation reached 890 W m^{-2} (days 190 and 193), while highest daily means were reached on days 192-194 (i.e., 303 W m^{-2}; 317 W m^{-2} and 300 W m^{-2}, respectively). Figure 3a also shows incoming longwave radiation. Incoming longwave radiation was relatively stable (~ 400 W m^{-2}) throughout the day and night of overcast days (e.g., day 187; daily mean of 403 W m^{-2}), at a time where peak daytime solar radiation was low 232 W m^{-2} (daily mean of 60 W m^{-2}). Incoming longwave radiation followed a diel cycle (between 280 W m^{-2} and 380 W m^{-2}; with mean values of 330 W m^{-2}) on clear days (e.g., days 192-194). These results show that daily mean values of incoming longwave radiation during clear days were generally lower than those during overcast days (330 W m^{-2} vs. 403 W m^{-2}; see above).

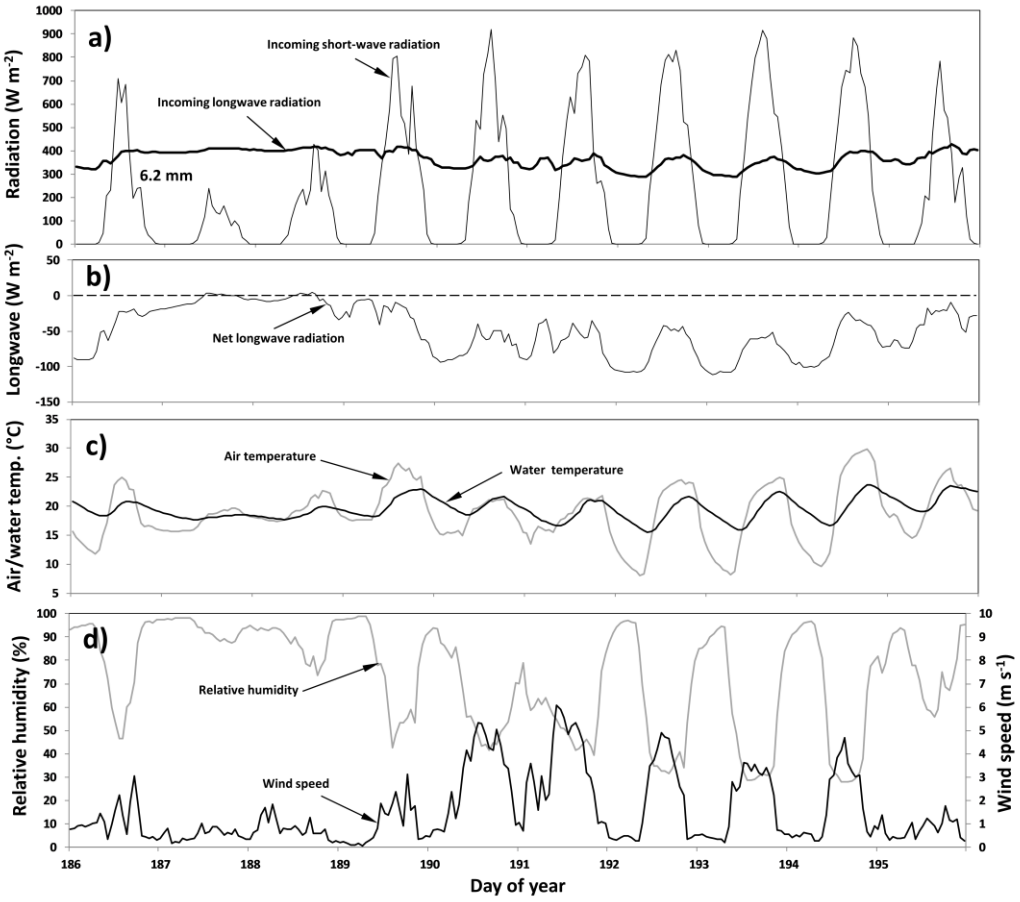

Figure 3. Microclimate conditions at the study site for the heat budget analysis and for the period of July 4 (day 186) to July 13 (day 195), 2012. Panels show the daily variation in a) incoming short- and longwave radiation, and b) net longwave radiation, highlighting how the longwave radiation is influenced by c) the water temperature. Panel c) also highlights the time lag between air and water temperature variations. Panel d) shows the daily variation in relative humidity and wind speed, which ultimately influence the daily variation in the latent flux.

Table 1. Little Southwest Miramichi River meteorological conditions between July 4 to July 13, 2012 (day 186-195).

Month	Day	Day of year	Meteorological conditions
July	4	186	Mainly clear, then mostly cloudy followed by rain showers (evening)
	5	187	Rain showers followed by cloudy, drizzle and fog conditions
	6	188	Cloudy, drizzle and fog throughout the day
	7	189	Fog in the morning followed by cloudy (mid-day) and clear condition (evening)
	8	190	Mainly clear for the first half of the day followed by mostly cloudy conditions
	9	191	Mostly cloudy then clear in the evening

10	192	Clear and mainly clear throughout the day
11	193	Clear and mainly clear throughout the day
12	194	Mainly clear followed by mostly cloudy and cloudy conditions
13	195	Coudly and mostly cloudy conditions throughout the day

Outgoing longwave radiation, calculated with equations 5 and 6, consisted mainly of radiation emitted by the water surface and a small reflected portion. Daily mean values were generally around 400 W m^{-2}, which included a small reflected portion of atmospheric incoming longwave radiation (~ 11 W m^{-2}). Figure 3b shows the net longwave radiation (incoming – outgoing), which was generally neutral (close to 0 W m^{-2}) during cloudy days (days 187-188; mean of -7 W m^{-2}). However, the net longwave radiation was a heat loss during clear days (daily average of -80 W m^{-2}, and reached night-time minimum values of -100 W m^{-2} on days 192-193). Figure 3c shows both air and water temperature during this period. Air and water temperature showed diel cycles during both cloudy and sunny/clear sky days. During sunny days, air and water temperatures can increase/decrease rapidly by the hour (e.g., days 192-194). Air temperature experienced the highest increase between 8:00 and 11:00 at rates of 3-3.2°C $h^{-1,}$ whereas water temperature showed the highest increase between 11:00 and 14:00 (slightly delayed) with rates of 0.8-0.9°C h^{-1}. The cooling rates of air temperatures (highest values) were similar to the heating rates (cooling of 3.2°C h^{-1} and occurred between 21:00 hrs and 23:00); however, water temperatures experienced lower cooling rates. Highest cooling rates for water temperatures were 0.55°C h^{-1} between 21:00 and 23:00, followed by relatively stable night-time cooling rates of 0.44°C hr^{-1} between midnight and 7:00. The cooling rates of water temperatures were about half in magnitude of water temperatures warming rates.

Figure 3d shows the relative humidity and wind speeds observed during the period of July 4 to 13 (days 186-195). Wind speeds were generally low during the beginning of the period (i.e., during cloudy and rainy days) and increased on days 190 and 191 (with peak values of 5.3 m s^{-1} and 6.0 m s^{-1}

on these days, respectively). The relative humidity was high during the beginning of the period (> 75%), especially during overcast days, and showed low diel variability; however, the diel variability increased during sunny days. During such days, the relative humidity varied between 28-32% (mid-day) to 95-97% (early morning; Figure 3d). Lowest relative humidity corresponded with highest wind speed conditions on those days.

3.2 Stream surface and streambed heat fluxes

Figure 4a shows the corresponding stream surface and streambed heat fluxes during the study period, i.e., July 4 to 13, 2012 (days 186 to 195). In Figure 4a, the solar radiation represents the net shortwave radiation, i.e., the measured incoming shortwave radiation minus the reflected component at 3% (of incoming). The net longwave radiation is the same time series as in Figure 3b (incoming – outgoing). Also shown in this figure are the sensible, the streambed, and the evaporative heat fluxes. Results show that all fluxes were relatively low during cloudy days (e.g., days 187-188) with correspondingly low diel variability. In contrast, surface heat fluxes were much higher during sunny days (e.g., days 192-194) with relatively high diel variability. The average net shortwave radiation was 206 W m^{-2} during this 10-day period and the only heat gain among all fluxes (mean value). All other fluxes over the 10-day period were heat losses (mean value). The evaporative heat flux represented the highest heat loss (average of -97 W m^{-2} and accounting for 48% of heat losses), followed by the net longwave radiation (-51 W m^{-2}; 25%), the streambed heat flux (-41 W m^{-2}; 20%) and the sensible heat flux (-12 W m^{-2}; 6%).

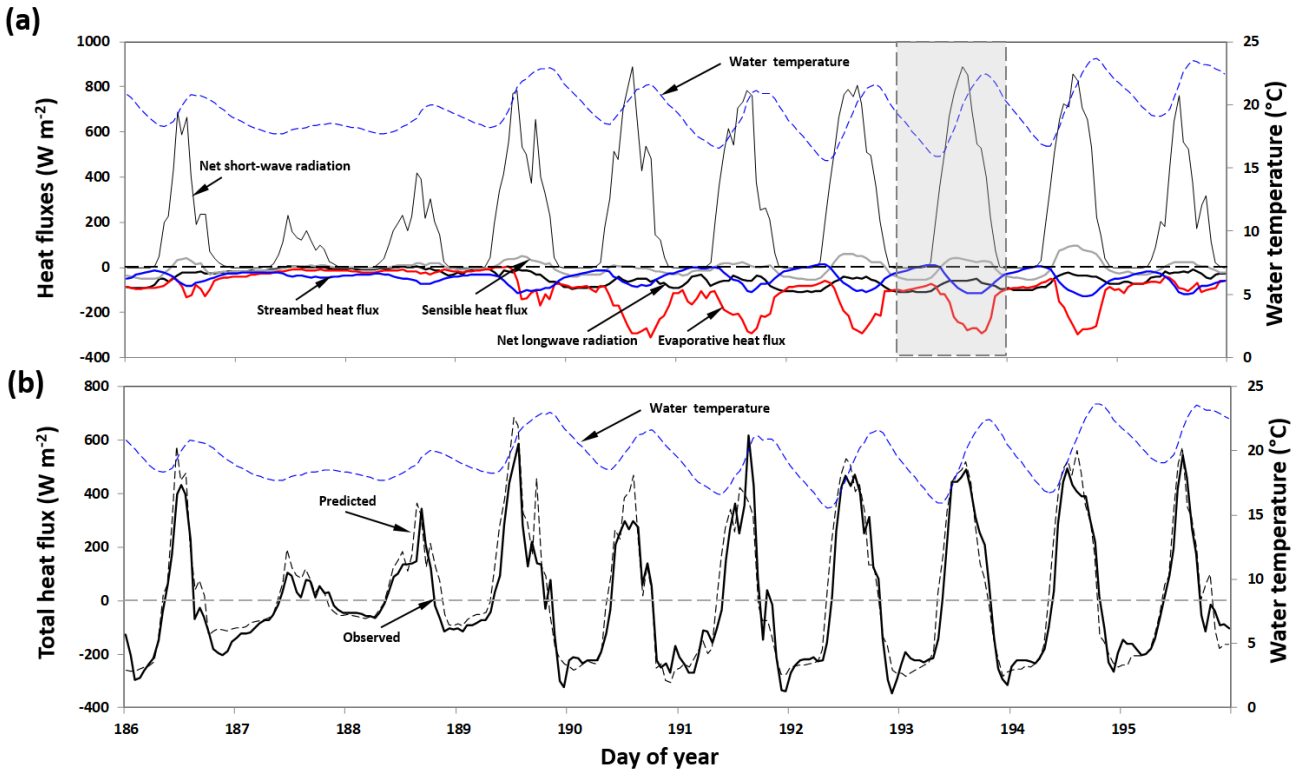

Figure 4. Calculated (a) heat fluxes (net short- and longwave radiation, streambed, sensible, and evaporative) and (b) total predicted and observed heat flux between July July 4 (day 186) and July 13 (day 195), 2012. Water temperature values are also displayed in both panels to show the variations in relation to the different heat fluxes.

When analyzing data over shorter time periods (e.g., cloudy and sunny days), a greater contrast between fluxes was observed. For instance, the net shortwave radiation, although relatively low, was still the most significant heat gain (89 W m^{-2}; daily mean values) during cloudy/overcast days (i.e., days 187-188; Figure 4a) where other fluxes were mainly heat losses. During these two days, the most significant heat loss was the streambed heat flux (-32 W m^{-2}; 54%), followed by the evaporative heat flux (-20 W m^{-2}; 34%), the net longwave radiation (-7 W m^{-2}; 12%), and sensible heat flux (close to 0 W m^{-2}). During sunny/clear sky days (day 192-194), the most significant heat gain was the shortwave radiation at 306 W m^{-2} (daily mean values), followed by a small contribution of sensible heat (2 W m^{-2}).

The most important heat loss during sunny days was the evaporative heat flux at -151 W m^{-2} (daily mean values; 56% of the heat losses), followed by the net longwave radiation (-76 W m^{-2}; 28%) and the streambed heat flux (-41 W m^{-2}; 15%). Both the evaporative heat flux and the net longwave radiation were important heat losses during sunny days; however, peak net longwave radiation losses occurred mainly at night (0:00-5:00 with values between -100 W m^{-2} and -110 W m^{-2}), while peak evaporative heat losses occurred in late afternoon (15:00 -18:00 with values between -290 W m^{-2} and -310 W m^{-2}; Figure 4a; peak value of -310 W m^{-2} occurred on day 190 at 18:00). The timing of the streambed heat flux was very close to that of the evaporative heat flux where maximum values occurred mainly in early morning, and minimum values occurred in late afternoon.

Figure 4b shows the corresponding predicted total heat flux calculated from the above total surface and streambed heat fluxes, i.e., calculated using the following equation:

$$H_{predicted} = H_{sw} + H_{lw} + H_{sh} + H_{evp} + H_{cond} \quad (13)$$

where the predicted total heat flux represents the summation of all heat fluxes, as calculated in Figure 4a. The observed total heat flux was obtained from actual changes in water temperatures over time (i.e., from measured water temperatures), given by the following equation:

$$H_{observed} = \frac{\rho_w \, c_w \, y \, \Delta T}{\Delta t} \quad (14a)$$

$$H_{observed} = 1163 \; y \, \Delta T \quad (14b)$$

where ρ_w and c_w represent the physical properties of water (as defined in equation 1), y represents the mean depth of water, and ΔT represents the actual measured changes in water temperatures over a 1-

hour period, i.e., Δt = 3600s. As such, equation 14b represents the energy required (W m^{-2}) to increase (or decrease) the water temperature by ΔT over a 1-hour period for the given depth y. Figure 4b shows both predicted (equation 13) and observed (equation 14) total heat fluxes. Predicted vs. observed total heat fluxes were very similar during the study period (days 186-195). Total maximum heat flux reached over 600 W m^{-2} (around 12:00-14:00), corresponding to a peak in net shortwave radiation input. The peak heat loss occurred towards the end of the day, around 22:00-23:00, with values reaching -350 W m^{-2}. Predicted heat fluxes (dashed line; Figure 4b) showed a slight lag to observed values from early morning to peak total fluxes (early afternoon).

Results for the overall study period, i.e., 87 days (between June 12, 2012, and September 6, 2012; day 164 and day 250), showed a similar fit of total heat fluxes (predicted vs. observed) with a root mean square error (*RMSE*) of 85 W m^{-2} and a coefficient of determination R^2 of 0.88 (Figure 5). This figure shows a slightly larger scatter for positive heat flux, with a few data points being far from the regression line. A closer look at some of these data points revealed that a rapid change in incoming solar radiation can explain some of this variability. For instance, on August 13:00 at 15:00 (point A; Figure 5), a marked variability in solar radiation was observed over a 3-hour period (767 W m^{-2}; 275 W m^{-2} and 758 W m^{-2}) where most other fluxes were relatively small and stable (< ±70 W m^{-2}). The water temperature increased by only 0.1°C during the last hour (15:00), which resulted in an observed total heat flux of 55 W m^{-2} ($H_{observed}$ = 1163 $y\,\Delta T$; water depth y = 0.47 m; equation 14b), where the predicted total heat flux ($H_{predicted}$) was calculated at 631 W m^{-2}, mainly as a result of the high solar radiation input of 758 W m^{-2} at 15:00. These results suggest that highly variable meteorological conditions at the hourly timescale are most likely responsible for such a difference between predicted and observed total flux.

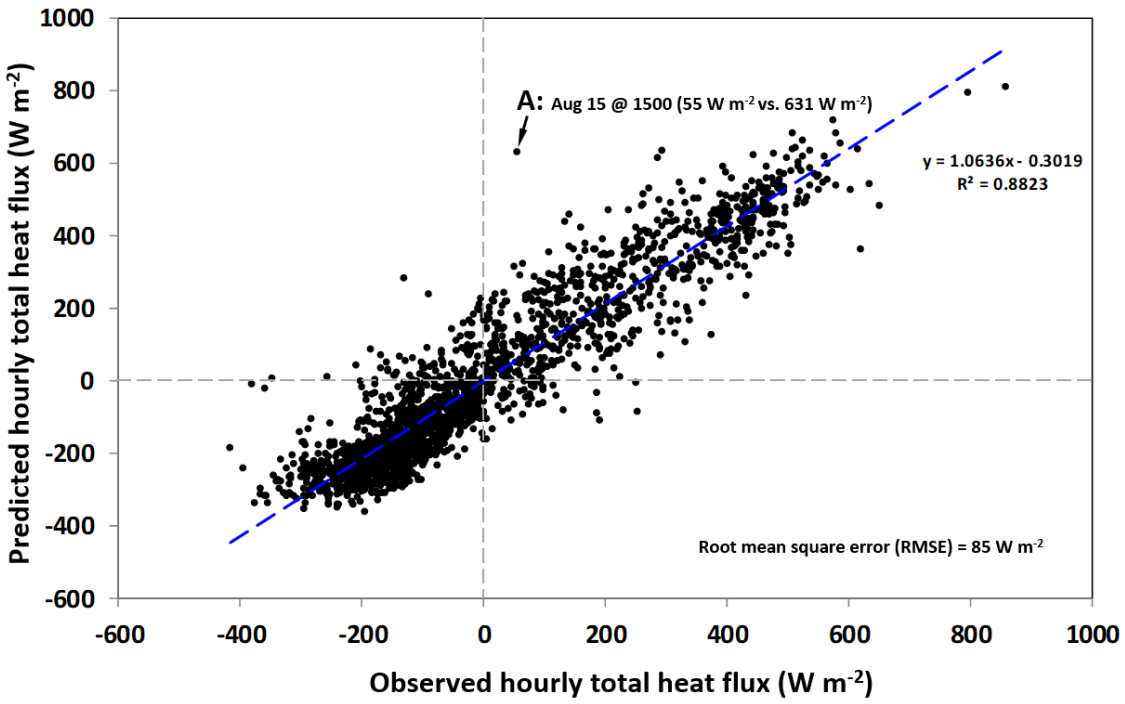

Figure 5. Observed vs. predicted latent heat flux using the Dalton-type approach equation.

3.3 Diel variability in river heat fluxes

A closer look at the timing of different heat fluxes during a 24-hour period is presented in Figure 6 (day 193; see shaded area, Figure 4a). This day (July 11; day 193) represents a typical clear day for the Little Southwest Miramichi River (i.e., mainly clear day; Table 1). On this day, water temperatures decreased gradually throughout the night and reached a minimum value of 15.9°C in the morning (9:00), and then increased to a maximum value of 22.5°C early evening (19:00). Air temperature followed a similar pattern with a minimum temperature of 8.1°C (6:00) and a maximum temperature of 25.0°C (19:00). Most heat fluxes throughout the night were stable until shortwave radiation increased at 7:00 (departure from zero of nightly values). Nighttime longwave radiation averaged -108 W m^{-2} (std = 2 W m^{-2}) followed by the evaporative heat flux (-91 W m^{-2}; std = 11 W m^{-2}), sensible heat flux (-52 W m^{-2}; std = 4 W m^{-2}) and the streambed heat flux (-5 W m^{-2}; std = 12 W m^{-2}). Both sensible heat and longwave

radiation increased during the day. Sensible heat peaked at 12:00 hrs (43 W m^{-2}), and longwave radiation reach its maximum value at 17:00 (-52 W m^{-2}). In contrast, both the streambed and evaporative heat fluxes reached their maximum early morning (streambed = 11 W m^{-2} and evaporative heat flux = -72 W m^{-2}), and then decreased during the daytime. Minimum values of both the streambed and the evaporative heat fluxes occurred around 18:00 (streambed = -114 W m^{-2} and evaporative flux = -293 W m^{-2}). During this time of day (1800 hrs), the net shortwave radiation (528 W m^{-2}) and sensible heat (27 W m^{-2}) represented heat gains, whereas longwave radiation (-68 W m^{-2}), streambed (-112 W m^{-2}), and the evaporative heat fluxes (-293 W m^{-2}) represented heat losses. The evaporative heat flux represented 62% of the total heat losses, representing the greater percentage of heat losses during the diel cycle when river temperatures reached maximum values. In fact, water temperatures reached peak values an hour later (19:00), and the evaporative heat flux still represented 61% of heat losses (latent heat flux = -278 W m^{-2} vs. total heat losses = -453 W m^{-2}). Notably, Figure 6 showed that the sensible heat and streambed heat fluxes showed both positive (gain) and negative values (loss), whereas the net longwave radiation and the evaporative heat fluxes were negative throughout the day.

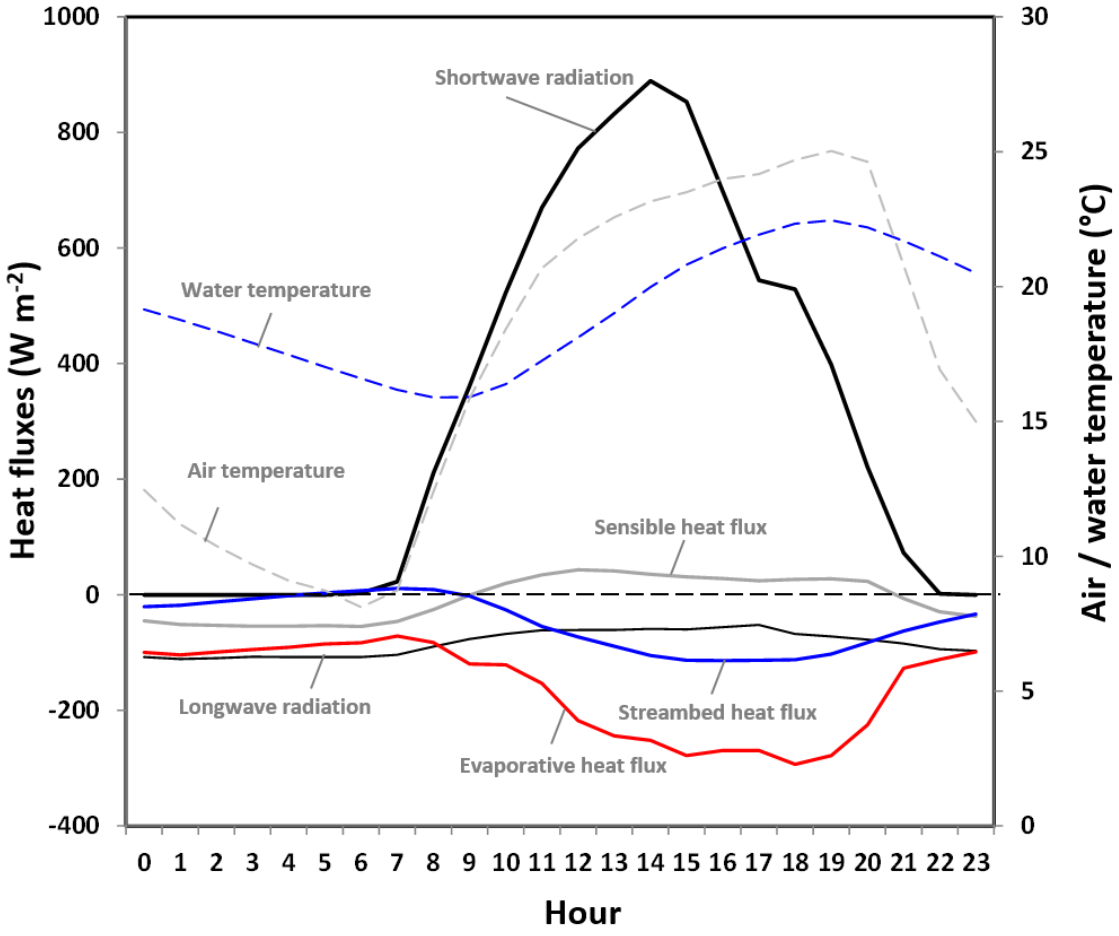

Figure 6. Timing of different heat fluxes and microclimate data at a hourly time step and for July 11 (day 193), 2012.

Figure 7 showed both daily and diel variability in the evaporative heat flux. Figure 7a shows the evaporative heat flux's minimum, maximum, and daily values during the study period. The daily evaporative heat flux varied between -204 W m^{-2} to 0 W m^{-2}. The evaporative heat flux reached positive values (heat gains) during a few days (day 179-182 and day 225-226), which were predominantly days of precipitation. The highest values of evaporative heat loss occurred during high water temperature events combined with relatively high wind speeds. For instance, a daily value of -204 W m^{-2} was recorded on day 219 (minimum value of -477 W m^{-2} at 17:00), where water temperature reached 27.8°C,

and wind speed was 4.6 m s^{-1}, with relative humidity less than 40%. During this high water temperature event, the net shortwave radiation (649 W m^{-2}) was the only heat gain, whereas all other fluxes were heat losses (evaporative heat fluxes = -477 W m^{-2}; longwave radiation = -80 W m^{-2}; sensible heat = -11 W m^{-2}; streambed = -129 W m^{-2}; total heat losses = -697 W m^{-2}). Notably, the evaporative heat flux represented 68% of the total heat losses during this day. We can calculate the hourly cooling component from the evaporative heat flux on this day using equation 14b (where the water depth was 0.3 m). As such, the hourly evaporative cooling for a corresponding evaporative heat flux of -477 W m^{-2} and a water depth of 0.3 m was calculated at 1.4 °C.

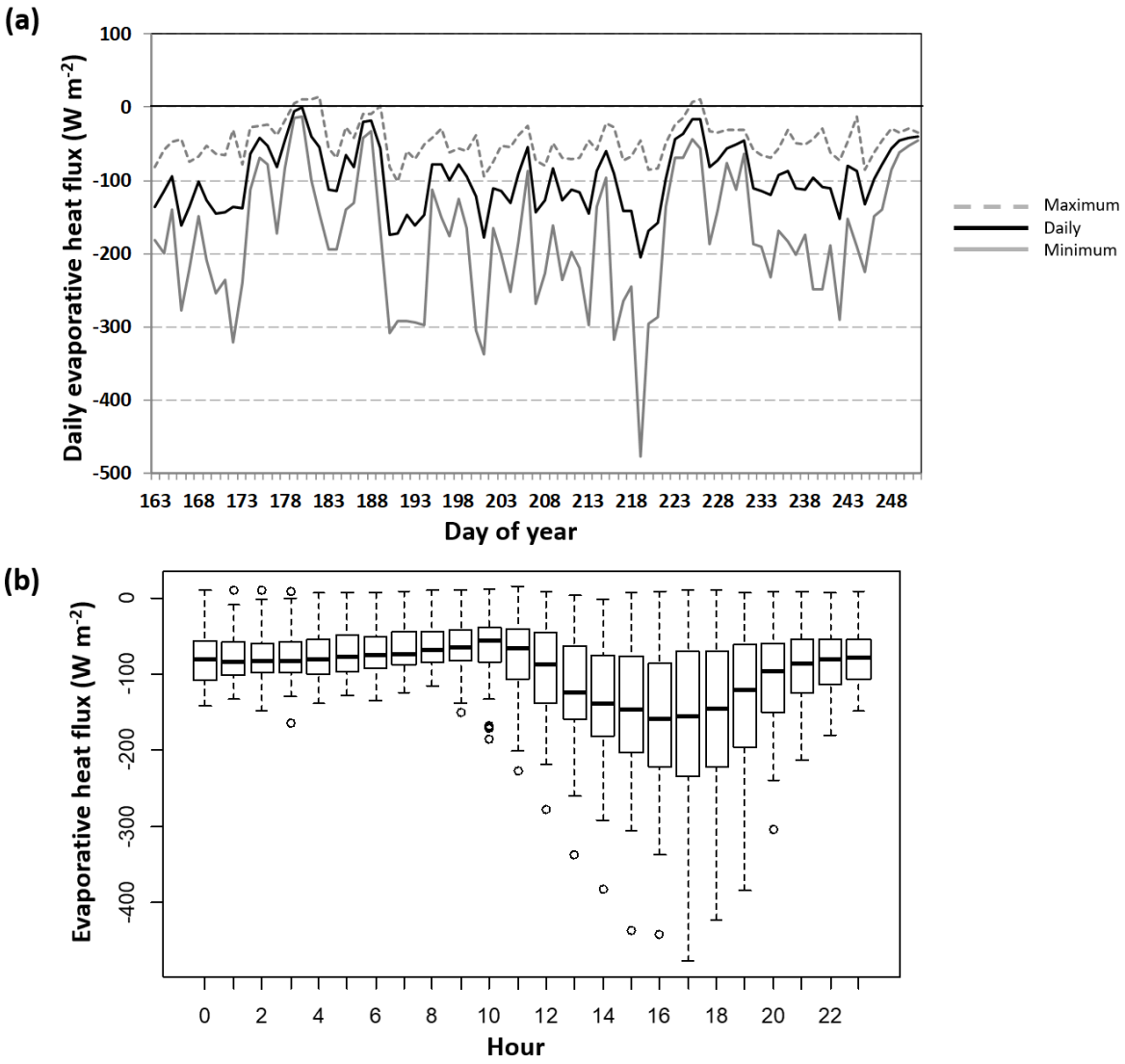

Figure 7. Daily and diel variability in the latent heat flux on the Little Southwest Miramichi River using in-situ meteorological data.

The diel pattern of the evaporative heat flux is presented in Figure 7b and shows that it was the major heat loss during the night (median values between -85 W m^{-2} and -74 W m^{-2}), and increased during the day to peak around 16:00-17:00. The maximum heat losses were mainly between 15:00 and 18:00, with median values -147 W m^{-2} (15:00), -160 W m^{-2} (16:00), -156 W m^{-2} (17:00), and -146 W m^{-2} (18:00). This is the time of day when river temperatures are generally reaching peak values. At between

150 W m^{-2} and 200 W m^{-2} (with a typical depth of 0.3 m), the evaporative cooling can be calculated at between 0.4°C and 0.5°C at the hourly timescale (equation 14b),

4. Discussion

Studies have highlighted the cooling effect of the evaporative heat flux in rivers, which can be particularly important during high summer temperatures (Benyahya et al. 2010; Maheu et al. 2014). The role and magnitude of the latent heat flux have received very little attention within the literature and remains generally poorly understood due to the difficulty of accurately measuring or modeling it. Since previous studies have shown important differences among site characteristics and wind function equations (e.g., Szeitz and Moore 2020), an in-river based equation for the wind function of the evaporative heat flux was used in the present study. Our results show that (1) the estimation of the evaporative heat flux can be improved with in-river/above water surface monitoring to better represent all fluxes and (2) that the evaporative heat losses can be very important for some rivers such as the Little Southwest Miramichi, i.e., river that are wide and shallow and experiencing relatively high river temperatures.

During the study period, the maximum water temperature reached 27.9°C; however, the Little Southwest Miramichi River can reach over 30°C during high summer water temperature events (Caissie et al. 2013). We showed that the evaporative heat flux can reach -300 Wm^{-2} to -450 W m^{-2} mid-day during high water temperatures (Figure 7), and these values can represent an hourly evaporative cooling around 1.4°C and account for 50%-68% of the total heat losses. The other heat losses are the longwave radiation (25%), followed by the streambed (20%), and sensible heat fluxes (5%). These results align with other studies showing that evaporative heat flux is an important source of energy loss at 30-40% of the total heat losses (Hebert et al. 2011; Webb and Zhang 2004). At close to 50% of the total heat losses (current study), the evaporative heat flux can be a critical cooling mechanism for wide and shallow

rivers during high summer temperatures as this study showed maximum evaporative cooling occurs at high temperatures.

Benner (2000) found that evaporation rates from John Day River in Oregon increased daily with the diurnal stream temperature increase. The present study showed similar patterns, with maximum evaporative heat flux losses generally happening during or a few hours before the timing of maximum daily stream temperature (which generally occurred a few hours after the maximum solar radiation input). These results confirm that the evaporative heat losses offset the net shortwave radiation and high river temperatures. This is an important finding as the net shortwave radiation is the dominant heat gain during the summer period, as also observed in previous studies (Hebert et al., 2011; Johnson 2004; Webb and Zhang, 1997; Webb and Zhang, 1999; Younus et al., 2000).

Previous studies have shown that different evaporative heat flux equations will yield very different results, especially if equations rely on using coefficients from the literature (e.g., Benyahya et al., 2010). It is worth mentioning that using fixed (constant) values for temperature-dependent coefficients (e.g., latent heat of water vaporization, water density, emissivity, etc.) have little impact on the predicted evaporative heat flux values (difference generally being $< 0.3\%$), given the uncertainties in the evaporation equation, especially the wind function. Furthermore, at hourly timescales, Dalton-type equations are the only equations available to calculate the evaporative heat flux, as energy-based equations (e.g., Priestley-Taylor or Penman) have been developed to be applied only at daily timescales (or longer timescales).

Data from land-based stations (often at the nearest airport) can show significant differences compared with data collected within the river environment, and thus land-based data may not truly capture river heat exchange processes, especially river evaporation. For instance, the evaluation of the radiative flux remains challenging. Longwave radiation re-emission can be easily estimated without

introducing uncertainties into the total heat budget (Maheu et al. 2014; Webb & Zhang, 1997), although in some settings, the accuracy of equipment may need to be taken into consideration (O'Sullivan and Kurylyk, 2020). The main challenge is that direct solar radiation inputs can be highly variable. It is also possible that the measured solar radiation at the instream meteorological station may not reflect the true solar radiation input experienced by the whole river. Indeed, our results suggest that during slightly cloudy days, the sun may hit (or not) the sensor or the river differently at different times of the day. Variances in radiative flux across time and scale have also been observed using remote sensing techniques, highlighting the potential of such technologies to provide data for better partitioning of river energy budgets (Richardson, Torgersen, and Moskal 2019; Dugdale 2016). Models development combining LiDAR data to inform on light penetration index with GIS-based solar models can now predict light regimes at the watershed scales with the same resolution that was previously possible for local point measurements (e.g., Bode et al. 2014), and could be used to further test spatial and temporal differences in solar loadings under different could regimes.

The river water temperature response time could also be a factor. For instance, between two hours of highly variable solar radiation, the water temperature response may have lagged slightly, thus influencing the observed total heat flux. These errors or uncertainties in the total heat flux calculations and water temperatures could also explain some of the differences observed in Figure 5. The Little Southwest Miramichi River depths ranged between 0.3 and 1 m, and on August 15, the water depth was 0.38 m. Equation 14b highlights that for a depth of 0.38 m, a heat flux of approximately 442 W m^{-2} is required to change the water temperature by 1°C. This also means that an error of 0.2°C in measured water temperatures would represent an error of 88 W m^{-2} in the total heat flux. As many water temperature sensors are within the range of ±0.2°C, errors representing 88 W m^{-2} could be expected in estimating the total heat flux. Finally, another limitation is that surface water interactions are in a

constant unsteady state, while it is possible for groundwater contributions to act as a buffer against surface heat gains.

One of the main issues with river evaporation is that very little is known on the universality of wind functions among rivers based on their position, the different landscape controls influencing convective patterns, and other factors that can lead to thermal inversions during hot summer days, ultimately impacting the evaporative heat flux. Many challenges of river environments contribute to this lack of knowledge, particularly monitoring river evaporation and different river size environments, i.e., sheltering and canopy closure, boundary-layer conditions, atmospheric stability, etc. Floating minipans have been used in recent studies and are showing promising results to better understand river evaporation processes. For instance, studies carried out within the Miramichi River (e.g., Maheu et al. 2014; Caissie 2016; Benyahya et al. 2010) and elsewhere (e.g. Benner 2000; Szeitz and Moore 2020) on different river sizes and sheltering characteristics seem to suggest that site-specific conditions can influence parameters of the wind function (e.g., canopy cover, river orientation, river incision, local topography). Therefore, it is important to gather more in-stream data to better understand the spatial and temporal variability of the evaporative heat flux. Results of the present study suggest that from a spatial perspective, evaporative cooling plays a major role in the overall river heat budget, by partially offsetting the incoming radiation heat flux. This is especially important for larger rivers and, more specifically, wide and shallow ones that experience elevated water temperature events. The results of our study highlight the importance of improving our understanding and modelling of the evaporative heat flux. This flux plays an important role in the overall river heat budget, especially for rivers in warmer climates that already exceed 30°C during the summer.

5. Conclusion

Underestimating or overestimating the evaporative heat flux can lead to important errors in modelling water temperature dynamics. This flux most likely plays a significant role in attenuating high summer temperatures and can have important implications from a climate change perspective. Improving heat budget modelling is important from a management perspective, where many studies aim to understand future river thermal dynamics and how to manage warming habitats of cold water sensitive species such as salmonids. For instance, data suggests that wide, shallow and highly exposed river (unsheltered) are those rivers that are currently reaching extreme temperatures (~ 30°C) within the salmonid habitat rivers. A better understanding and modelling of the evaporative heat flux could be used to improve mitigation designs aiming at protecting rivers against excessive heating (e.g., maintaining riparian buffer zones along river, tree planting, protecting cold-water habitat, etc.). These actions are particularly essential for cold water fish species, so they can access a mosaic of thermal habitats allowing them to maximize their growth while accessing cold water refuges that provide physiological relief during high summer thermal events.

ACKNOWLEDGEMENTS

We thank Dr. Audrey Maheu for her help in meteorological data collection. We are also thankful for the constructive comments from one anonymous reviewer, from Graham Goulette (NOAA) and Antóin O'Sullivan (University of New-Brunswick).

Conflict of interests

The authors have no conflict of interest to declare

Data availability

This paper presents all data used for the heat fluxes calculations directly.

REFERENCES

Ahmadi-Nedushan B, St-Hilaire A, Ouarda TBMJ, Bilodeau L, Robichaud E, Thiémonge N, Bobée B. 2007. Predicting river water temperatures using stochastic models: case study of the Moisie River (Québec, Canada). *Hydrological Processes* **21**: 21-34.

Anderson ER. 1954. Energy-budget studies, water-loss investigations: Lake Hefner studies. *US Technical report, Professional Paper 269*, Geological Survey, US Department of Interior, Washington, DC, pp. 71–119.

Armstrong, Jonathan B, Daniel E Schindler, Casey P Ruff, Gabriel T Brooks, Kale E Bentley, and Christian E Torgersen. 2013. Diel Horizontal Migration in Streams: Juvenile Fish Exploit Spatial Heterogeneity in Thermal and Trophic Resources. *Ecology* 94 (9): 2066–75. https://doi.org/10.1890/12-1200.1.

Benner, David A. 2000. Evaporative Heat Loss of the Upper Middle Fork of the John Day River, Northeastern Oregon. *Thesis*. Oregon State University.

Benyahya L, Caissie D, El-Jabi N, Satish MG. 2010. Comparison of microclimate vs. remote meteorological data and results applied to a water temperature model (Miramichi River, Canada). *Journal of Hydrology* **380**: 247–259.

Benyahya L, Caissie D, Satish MG, El-Jabi N. 2012. Longwave radiation and heat flux estimates within a small tributary in Catamaran Brook (New Brunswick, Canada). *Hydrological Processes* **26**: 475-484.

Bode, Collin A., Michael P. Limm, Mary E. Power, and Jacques C. Finlay. 2014. Subcanopy Solar Radiation Model: Predicting Solar Radiation across a Heavily Vegetated Landscape Using LiDAR and GIS Solar Radiation Models. *Remote Sensing of Environment* 154: 387–97. https://doi.org/10.1016/j.rse.2014.01.028.

Bowen IS. 1926. The ratio of heat losses by conduction and by evaporation for any water surface. *Phys. Rev*. **27**: 316–355.

Breau, Cindy, Richard A. Cunjak, and Stephan J. Peake. 2011. Behaviour during Elevated Water Temperatures: Can Physiology Explain Movement of Juvenile Atlantic Salmon to Cool Water? *Journal of Animal Ecology* 80 (4): 844–53. https://doi.org/10.1111/j.1365-2656.2011.01828.x.

Caissie, Daniel, and Charles H. Luce. 2017. Quantifying Streambed Advection and Conduction Heat Fluxes." *Water Resources Research* 53 (2): 1595–1624. https://doi.org/10.1002/2016WR019813.

Caissie, D, El-Jabi, N, and Turkkan, N. 2014. Stream Water Temperature Modeling Under Climate Change Scenarios - Phase II: Study of Stream Water Temperatures Under Climate Change Scenarios B1 & A2. *Can. Tech. Rep. Fish. Aquat. Sci. 3106: ix + 51p.*

Caissie D, Kurylyk BL, St-Hilaire A, El-Jabi N, MacQuarrie KTB. 2014. Streambed temperature dynamics and corresponding heat fluxes in small streams experiencing seasonal ice cover. Journal of Hydrology **519**: 1441-1452.

Caissie D, Breau C, Hayward J, Cameron P. 2013. Water temperature characteristics within the Miramichi and Restigouche rivers, *DFO Can. Sci. Advis. Sec. Res. Doc*. 2012/165. vi + 31 p.Caissie D, El-Jabi N. 1995. Hydrology of the Miramichi River drainage basin, *In:* Water, science, and the public: the Miramichi ecosystem, Chadwick EMP (eds). Canadian Special Publication of Fisheries and Aquatic Sciences: Ottawa, Canada, 123 pp. 83–93.

Caissie D. 2011. The design of a new device to automate a Class A evaporation pan, *Can. Tech. Rep. Fish. Aquat. Sci.* 2927: vii + 33p.

Caissie D, Satish MG, El-Jabi N. 2007. Predicting water temperatures using a deterministic model: Application on Miramichi River catchments (New Brunswick, Canada). *Journal of Hydrology* **336**(3): 303–315.

Caissie D. 2006. The thermal regime of rivers: A review. *Freshwater Biology* **51:** 1389-1406.

Caissie, D, El-Jabi, N, Satish, MG. 2001. Modelling of maximum daily water temperatures in a small stream using air temperatures. *J. Hydrol.* 251, 14–28. doi: 10.1016/S0022-1694(01)00427-9.

Caissie, D., Satish, M.G., 2001. Modelling water temperatures at depths within the stream substrate at Catamaran Brook (NB): potential implication of climate change. Can Tech. Rep. Fish. Aquat. Sci. 2365, 27p.

Caissie, D. and El-Jabi, N. 1995 Hydrology of the Miramichi River Drainage Basin. In: Chadwick, E.M.P., Ed., Water, Science, and the Public: The Miramichi Ecosystem. NRC Research Press, Ottawa, 83-93.

Carrivick, Jonathan L., Lee E. Brown, David M. Hannah, and Andy G D Turner. 2012. Numerical Modelling of Spatio-Temporal Thermal Heterogeneity in a Complex River System. *Journal of Hydrology* 414–415: 491–502. https://doi.org/10.1016/j.jhydrol.2011.11.026.

Cluis DA. 1972. Relationship between stream water temperature and ambient air temperature - A simple autoregressive model for mean daily stream water temperature fluctuations. *Nordic Hydrology* **3**(2): 65-71.

Corey, Emily, Tommi Linnansaari, Richard A. Cunjak, and Suzanne Currie. 2017. Physiological Effects of Environmentally Relevant, Multi-Day Thermal Stress on Wild Juvenile Atlantic Salmon (Salmo Salar). *Conservation Physiology* 5 (1): 1–13. https://doi.org/10.1093/conphys/cox014.

Cunjak RA, Linnansaari T, Caissie D. 2013. The complex interaction of ecology and hydrology in a small catchment: a salmon's perspective. *Hydrological Processes* **27**: 741-749.

Dugdale, Stephen J., David M. Hannah, and Iain A. Malcolm. 2017. River Temperature Modelling: A Review of Process-Based Approaches and Future Directions. *Earth-Science Reviews* 175 (October): 97–113. https://doi.org/10.1016/j.earscirev.2017.10.009.

Dugdale, Stephen J. 2016. "A Practitioner's Guide to Thermal Infrared Remote Sensing of Rivers and Streams: Recent Advances, Precautions and Considerations." *Wiley Interdisciplinary Reviews: Water* 3: 251–68. https://doi.org/10.1002/wat2.1135.

Dugdale, Stephen J., Normand E. Bergeron, and André St-Hilaire. 2015. Spatial Distribution of Thermal Refuges Analysed in Relation to Riverscape Hydromorphology Using Airborne Thermal Infrared Imagery. *Remote Sensing of Environment* 160: 43–55. https://doi.org/10.1016/j.rse.2014.12.021.

Elvidge, C K, E L L Cooke, R A Cunjak, and S J Cooke. 2017. Social Cues May Advertise Habitat Quality to Refuge-Seeking Conspecifics Canadian Journal of Zoology (5): 1–5. https://doi.org/10.1139/cjz-2016-0144.

Frechette, Danielle M., Stephen J Dugdale, Julian J Dodson, and Normand E Bergeron. 2018. Understanding Summertime Thermal Refuge Use by Adult Atlantic Salmon Using Remote Sensing, River Temperature Monitoring, and Acoustic Telemetry. *Canadian Journal of Fisheries and Aquatic Sciences* 12: 1999-2010, cjfas-2017-0422. https://doi.org/10.1139/cjfas-2017-0422.

Fulford JM, Sturm TW. 1984. Evaporation from flowing channels. *Journal of Environmental Engineering* **110**(1): 1-9.

Garner, G, I A Malcolm, J P Sadler, and D M Hannah. 2014. What Causes Cooling Water Temperature Gradients in a Forested Stream Reach? *Hydrology and Earth System Sciences* 18: 5361–76. https://doi.org/10.5194/hess-18-5361-2014.

Guenther SM, Moore RD, Gomid T. 2012. Riparian microclimate and evaporation from a coastal headwater stream, and their response to partial-retention forest harvesting. *Agricultural and Forest Meteorology* **164**: 1– 9.

Gulliver JS, Stefan HG. 1986. Wind function for a sheltered stream. *Journal of Environmental Engineering* **112**(2): 387-399.

Hannah DM, Malcolm IA, Soulsby C, Youngson AF. 2008. A comparision of forest and moorland stream microclimate, heat exchanges and thermal dynamics. *Hydrological Processes* **22**: 919-940.

Hare, D. k., A. m. Helton, Z. C. Johnson, J. W. Lane, and M. A. Briggs. 2021. Groundwater Contributions to Streams. *Nature Communications*, no. 12: 1450. http://dx.doi.org/10.1038/s41467-021-21651-0.

Hebert C, Caissie D, Satish MG, El-Jabi N. 2011. Study of stream temperature dynamics and corresponding heat fluxes within Miramichi River catchments (New Brunswick, Canada). *Hydrological Processes* **25**: 2439–2455. https://doi:10.1002/hyp.8021

Hockey JB, Owens IF, Tapper NJ. 1982. Empirical and theoretical models to isolate the effect of discharge on summer water temperatures in the Hurunui River. *Journal of Hydrology (New Zealand)* **21**: 1-12.

Huntsman, A. G. 1942. Death of Salmon and Trout with High Temperature. *Journal of the Fisheries Research Board of Canada* 5c (5): 485–501. https://doi.org/10.1139/f40-051.

Jackson, F. L., D. M. Hannah, V. Ouellet, and I. A. Malcolm. 2021. A Deterministic River Temperature Model to Prioritize Management of Riparian Woodlands to Reduce Summer Maximum River Temperatures. *Hydrological Processes* 35 (8): 1–19. https://doi.org/10.1002/hyp.14314.

Jobson, H. E.1980. "Thermal Modeling of Flow in the San Diego Aqueduct, California, and Its Relation to Evaporation." USGS Professional Paper #1122. US Department of Interior, Washington, DC.
31 p. https://doi.org/10.3133/pp1122.Johnson, S. L. 2004. Factors Influencing Stream Temperatures in Small Streams: Substrate Effects and a Shading Experiment. *Canadian Journal of Fisheries and Aquatic Sciences* 61 (6): 913–23. https://doi.org/10.1139/f04-040.

Keefer, M. L., C. a. Peery, and B. High. 2009. Behavioral Thermoregulation and Associated Mortality Trade-Offs in Migrating Adult Steelhead (Oncorhynchus Mykiss): Variability among Sympatric Populations. *Canadian Journal of Fisheries and Aquatic Sciences* 66 (10): 1734–47. https://doi.org/10.1139/F09-131.

Kingsolver, Joel G., Sarah E. Diamond, and Lauren B. Buckley. 2013. Heat Stress and the Fitness Consequences of Climate Change for Terrestrial Ectotherms. *Functional Ecology* 27 (6): 1415–23. https://doi.org/10.1111/1365-2435.12145.

Kurylyk, Barret L., Kerry T.B. Macquarrie, Tommi Linnansaari, Richard A. Cunjak, and R. Allen Curry. 2015. Preserving, Augmenting, and Creating Cold-Water Thermal Refugia in Rivers: Concepts Derived from Research on the Miramichi River, New Brunswick (Canada). *Ecohydrology* 8 (6): 1095–1108. https://doi.org/10.1002/eco.1566.

Leach, Jason A, and R Dan Moore. 2018. Empirical Stream Thermal Sensitivities May Underestimate Stream Temperature Response to Climate Warming. https://doi.org/10.1029/2018WR024236.

Leach JA, Moore RD. 2010. Above-stream microcliamte and stream surface energy exchanges in a wildfire-disturbed riparian zone. *Hydrological Processes* 24: 2369-2381.

Lowney CL. 2000. Stream temperature variation in regulated rivers: Evidence for a spatial pattern in daily minimum and maximum magnitudes. *Water Resources Research* **36**(10): 2947-2955.

Maheu A, Caissie D, St-Hilaire A, El-Jabi N. 2014. River evaporation and corresponding heat fluxes in forested catchments. *Hydrological Processes* **28**: 5725-5738.

McJannet DL, Webster IT, Cook FJ. 2012. An area-dependent wind function for estimating open water evaporation using land-based meteorological data. *Environmental Modelling & Software* **31**: 76-83.

Mohseni, O, and H G Stefan. 1999. Stream Temperature/Air Temperature Relationship: A Physical Interpretation. *Journal of Hydrology* 218 (3–4): 128–41. https://doi.org/10.1016/S0022-1694(99)00034-7.

Ouellet, V. and M. D. Daniels. 2021. Brook Trout (Salvelinus Fontinalis) and Brown Trout (Salmo Trutta) Summer Thermal Habitat Use in Streams with Sympatric Populations. *Journal of Thermal Biology* 98 (January 2020): 102931. https://doi.org/10.1016/j.jtherbio.2021.102931.

Ouellet, V., A. St-hilaire, S. J Dugdale, D. M Hannah, S. Krause, and S. Ouellet-P. 2020. River Temperature Research and Practice : Recent Challenges and Emerging Opportunities for Managing Thermal Habitat Conditions in Stream Ecosystems. *Science of the Total Environment* 736. https://doi.org/10.1016/j.scitotenv.2020.139679.

Ouellet, V., Y. Secretan, A. St-Hilaire, and J.Morin. 2014. Water Temperature Modelling in a Controlled Environment: Comparative Study of Heat Budget Equations. *Hydrological Processes* 28 (2): 279–92. https://doi.org/10.1002/hyp.9571.

Ouellet, V., Y. Secretan, A. St-Hilaire, and J. Morin. 2013. Daily Averaged 2D Water Temperature Model for the St. Lawrence River. *River Research and Applications* 30: 733–44. https://doi.org/10.1002/rra.

Ouellet, V., M. Mingelbier, A. Saint-Hilaire, and J. Morin. 2010. ".Frequency Analysis as a Tool for Assessing Adverse Conditions during a Massive Fish Kill in the St. Lawrence River, Canada. *Water Quality Research Journal of Canada* 45 (1): 47–57. https://doi.org/10.2166/wqrj.2010.006.

O'Sullivan, A. M., and B. L. Kurylyk. 2022. Limiting External Absorptivity of UAV-Based Uncooled Thermal Infrared Sensors Increases Water Temperature Measurement Accuracy. *Remote Sensing* 14, no. 24: 6356. https://doi.org/10.3390/rs14246356

O'Sullivan, A. M., K. J. Devito, J.Ogilvie, T. Linnansaari, T. Pronk, S. Allard, and R. A.Curry. 2020. "Effects of Topographic Resolution and Geologic Setting on Spatial Statistical River Temperature Models." *Water Resources Research* 56 (12): 1–23. https://doi.org/10.1029/2020WR028122

O'Sullivan, A. M., K. J Devito, and R. A. Curry. 2019. The Influence of Landscape Characteristics on the Spatial Variability of River Temperatures. *Catena* 177 (March 2018): 70–83. https://doi.org/10.1016/j.catena.2019.02.006.

Palmer, Margaret A, and K.C. Nelson. 2007. Stream Temperature Surges Under Urbanization and Climate Change. *Journal Of The American Water Resources Association* 43 (2): 440–52. https://doi.org/10.1111/j.1752-1688.2007.00034.x.

Petty, J. Todd, David Thorne, Brock M. Huntsman, and Patricia M. Mazik. 2014. The Temperature-Productivity Squeeze: Constraints on Brook Trout Growth along an Appalachian River Continuum. *Hydrobiologia* 727 (1): 151–66. https://doi.org/10.1007/s10750-013-1794-0.

Richardson, J. J., C. E. Torgersen, and L. M. Moskal. 2019. "Lidar-Based Approaches for Estimating Solar Insolation in Heavily Forested Streams." *Hydrology and Earth System Sciences* 23 (7): 2813–22. https://doi.org/10.5194/hess-23-2813-2019.

River, J., A. Curry, A. St-hilaire, and S. N Andrews. 2018. Impact of Future Climate Change on Water Temperature and Thermal Habitat for Keystone Fishes in the Lower Saint. https://doi.org/10.1007/s11269-018-2057-7.

Sinokrot BA, Stefan HG. 1993. Stream temperature dynamics: Measurements and modeling. *Water Resources Research* **29**(7): 2299-2312.

Svenning, Martin A., Morten Falkegård, J. Brian Dempson, Michael Power, Bård- Jørgen Bårdsen, Gudni Guðbergsson, and Per Fauchald. 2022. "Temporal Changes in the Relative Abundance of Anadromous Arctic Charr, Brown Trout, and Atlantic Salmon in Northern Europe: Do They Reflect Changing Climates?" *Freshwater Biology* 67 (1): 64–77. https://doi.org/10.1111/fwb.13693.

Szeitz, AJ, Moore, RD. Predicting evaporation from mountain streams. *Hydrological Processes*. 2020; 34: 4262– 4279. https://doi.org/10.1002/hyp.13875

Tague, Christina, I Michael Farrell, Gordon Grant, Sarah Lewis, and Serge Rey. 2007. Hydrogeologic Controls on Summer Stream Temperatures in the McKenzie River Basin, Oregon. *Hydrological Processes* 21: 3288–3300.

Troxler RW, Thackston EL. 1977. Predicting the rate of warming of rivers below hydroelectric installations. *Journal of Water Pollution Control Federation* **49**: 1902–1912.

Vercauteren N, Bou-Zeid E, Huwald H, Parlange MB, Brutsaert W. 2009. Estimation of wet surface evaporation from sensible heat flux measurements. *Water Resour. Res*., **45**, W06424, doi:10.1029/2008WR007544.

Webb, B.W. and Zhang, Y. 2004, Intra-annual variability in the non-advective heat energy budget of Devon streams and rivers. Hydrol. Process., 18: 2117-2146. https://doi.org/10.1002/hyp.1463

Webb, B.W. and Zhang, Y. 1999. Water temperatures and heat budgets in Dorset chalk water courses. Hydrol. Process., 13: 309-321. https://doi.org/10.1002/(SICI)1099-1085(19990228)13:3<309::AID-HYP740>3.0.CO;2-7

Webb BW, Zhang Y. 1997. Spatial and seasonal variability in the components of the river heat budget. *Hydrological Processes* **11**: 79-101.

Younus M, Hondzo M, Engel BA. 2000. Stream temperature dynamics in upland agricultural watershed. *Journal of Environmental Engineering* **126**(6): 518-526.